# ENERGY FLOW UNCERTAINTIES IN VIBRATING SYSTEMS: DEFINITION OF A STATISTICAL CONFIDENCE FACTOR

Antonio Culla and Aldo Sestieri

*Università degli Studi di Roma 'La Sapienza', via Eudossiana, 18-00184 Rome, Italy*
E-mail: aldo.sestieri@uniroma1.it

and

Antonio Carcaterra

*INSEAN, via di Vallerano, 139-00128 Rome, Italy*

A method for evaluating the energy flow confidence level in vibrating systems with randomly perturbed parameters is presented. The energy flow is predicted in terms of the mobilities of resonant subsystems or by the solution of the velocity wave field for non-resonant subsystems. The statistical moments of the energy flow are calculated by a perturbation technique and a confidence factor is defined as the ratio between mean and standard deviation. The properties of the confidence factor are investigated by a theoretical analysis as a function of frequency. Three cases are studied to compare the confidence factor obtained theoretically with a prediction provided by a Monte-Carlo simulation.

© 2003 Elsevier Science Ltd. All rights reserved.

## 1. INTRODUCTION

In studying high-frequency dynamic problems, two main difficulties must be considered. First, because of the small wavelengths involved, a large number of degrees of freedom is required to describe the field appropriately; second, inherent uncertainties of any of the physical, geometrical or joint parameters imply unpredictable (random) behaviours. The deterministic methods of analysis, such as finite element or boundary element methods, are not capable, in general, of overcoming such shortcomings. In fact, the large number of degrees of freedom makes the computational burden very heavy and, generally, not very accurate; moreover, a deterministic approach is not appropriate to analyse a problem that is so sensitive to small variations of the system parameters associated to the physical model. On the contrary, statistical energy methods are quite efficient for overcoming both the mentioned difficulties. On one hand the large set of degrees of freedom is simply replaced by few energy values; on the other hand, a more relevant statistical description of any parametrical uncertainty is considered [1].

For its intrinsic capacity of accounting for average quantities such as coupling loss factors and modal densities that depend on the area (length, volume) of the vibrating system, rather than on its geometrical details, the statistical energy analysis (SEA) is expected to be a statistical approach describing the average response of a population instead of the single sample response [1–6]. However, SEA only partially uses the strength of the statistical approaches. In fact, it only provides information on the first-order moments related to the energy of the system, but does not deal with the dispersion

information and does not provide any standard deviation of the results, although people involved with SEA recognise that this method is much more reliable at high frequencies and/or for systems with a high modal overlap. Actually, an attempt to estimate the dispersion information and the confidence in the results is given by Lyon [5]. However, his developments refer to a particular problem: he assumes that the natural frequencies occur randomly with a Poisson distribution and uses this probability density function to calculate the variance of the solution [5, 7]. This model holds only if very particular conditions are met, e.g. a constant modal density.

Aim of this paper is to provide the confidence levels for the energy and the energy flow between coupled structure under more general statistical conditions, i.e. when uncertainty exists in the physical parameters of the system. The analysis provides the statistics of the energies of the two coupled subsystems as well as of the energy flow between them. The analysis is not directly addressed to SEA applications. In fact, the space and frequency mean is not considered, whereas the statistical moments of the energy flow are calculated only considering a random population of similar systems. Moreover, this stochastic population is built by imposing a random perturbation only on some physical parameters of the studied sytems. However, this can be thought as a starting point for more general developments.

In particular, the following points are developed. Under the hypothesis of a small perturbation, the statistics of the energy flows among the systems are determined in closed form, whatever the probability density functions of the process. On the basis of this result, the characteristic trend of the energy flow dispersions are predicted for different strengths of coupling. To verify the obtained results a Monte-Carlo numerical simulation is performed on a significant number of realizations [8].

## 2. ENERGY FLOW ANALYSIS BETWEEN COUPLED DYNAMIC SYSTEMS

The goal of this paper is to study the mean and standard deviation of the vibrational energy flowing through dynamic systems having random characteristic parameters. To achieve this result the ratio between the mean and standard deviation of the energy flow, hereafter called confidence factor $f_c$, is examined in detail, as a tool able to quantify the uncertainty of the energy flow prediction. The expression 'dynamic system' indicates, in this paper, two possible kinds of system: resonators and wave guides.

The study is first addressed to the analysis of two multi-modal resonators coupled together by a joint having random stiffness. We will prove that the confidence factor presents two different frequency trends, separated by a transition frequency. Below the transition frequency the systems exhibits a modal behaviour; beyond it the effect of modes is negligible and the system is more appropriately described by a non-resonant wave guide.

The analysis is developed through the following three steps:

- calculation of the velocities and associated forces field,
- calculation of the energy flow depending on the random parameters of the system,
- study of the confidence factor.

A perturbation technique enables the calculation of the mean and standard of the energy flow deviation in terms of the random parameter of the system. Since the confidence factor is frequency dependent, the behaviour in the high-frequency range is studied by the limit:

$$\lim_{\omega \to \infty} f_c.$$

The following systems are considered:

1. resonator–joint with random stiffness–resonator
2. wave guide with random Young modulus
3. finite continuous system with random Young's modulus
4. wave guide with random Young modulus coupled with a resonator
5. wave guide–joint with random stiffness–wave guide.

Here we refer the resonator to a finite contiuous dynamic system. The analysis refers to a population with random physical parameters.

Since the analysis is similar for all the cases considered, we develop in detail the resonator–random joint–resonator system only while for the other cases, their relevant characteristics are presented and discussed.

### 3. ENERGY FLOW ANALYSIS BETWEEN TWO COUPLED RESONATORS WITH A RANDOM PERTURBATION ON THE JOINT PARAMETERS

Consider two resonators I and II (Fig. 1). Subsystem I is excited by a harmonic point force $f_1(t) = F_1 e^{j\omega t}$ (applied at point 1) and coupled to subsystem II by a linear massless joint III connecting the two resonators between points 2 and 3.

The general expression of the time-average power at the generic point $i$ is

$$P_i = \tfrac{1}{2}\mathrm{Re}\{F_i V_i^*\} \tag{1}$$

where $F_i$ and $V_i$ are the phasor of the force applied at $i$ and the velocity phasor at the same point, respectively, and '*' denotes complex conjugate [1]. Since the joint is massless, the coupling between I and II implies the continuity condition

$$F_2 = F_3. \tag{2}$$

The mobility relationships for system I are

$$v_1 = M_{11}F_1 - M_{12}F_2$$
$$v_2 = M_{21}F_1 - M_{22}F_2. \tag{3}$$

The mobility relationship for system II is

$$v_3 = M_{33}F_3 \tag{4}$$

and finally the additional mobility equation holds:

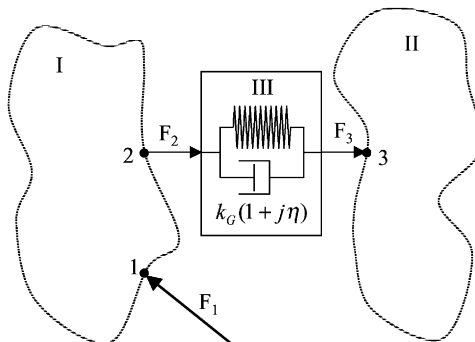$$v_2 = F_2(M_{33} + M_{\mathrm{III}}). \tag{5}$$



Figure 1. Resonator–random joint–resonator.

It is obtained considering the serial connection between III and II, where

$$M_{\text{III}} = \frac{\omega(\eta + j)}{k_G(\eta^2 + 1)}$$

$k_G$ being the joint stiffness and $\eta$ the loss factor.

The set of conditions (2)–(5) can be regarded as a system of five linear equations to be solved in terms of the five unknowns $v_1$, $v_2$, $v_3$, $F_2$, $F_3$, supposing that the external force $F_1$ and the whole set of mobilities $M_{ij}$ ($i, j = 1, 2$), $M_{33}$ and $M_{\text{III}}$ are known. Once the system is solved, the powers $P_2$ and $P_3$ take the form

$$P_3 = \frac{1}{2} \operatorname{Re}\{F_3 V_3^*\} = \frac{1}{2} \frac{|M_{21} F_1|^2}{|M_{33} + M_{22} + M_{\text{III}}|^2} \operatorname{Re}\{M_{33}^*\} \tag{6}$$

$$P_2 = \frac{1}{2} \operatorname{Re}\{F_2 V_2^*\} = -\frac{1}{2} \frac{|M_{21} F_1|^2}{|M_{33} + M_{22} + M_{\text{III}}|^2} \operatorname{Re}\{M_{33}^* + M_{\text{III}}\}. \tag{7}$$

It would be noted that equations (6) and (7) provide $P_2$ negative and $P_3$ positive consistently with the fact that $P_2$ is a power leaving system I, while $P_3$ is a power entering system II. Finally the power dissipated in the joint is:

$$P_{J\text{diss}} = -(P_2 + P_3).$$

Assuming $\eta \ll 1$, the term $\eta^2$ in $M_{\text{III}}$ can be neglected and equations (6) and (7) become

$$P_3 = \frac{1}{2} \frac{|M_{21} F_1|^2}{|M_{33} + M_{22} + \omega(\eta + j)/k_G|^2} \operatorname{Re}\{M_{33}^*\} \tag{8}$$

$$P_2 = -\frac{1}{2} \frac{|M_{21} F_1|^2}{|M_{33} + M_{22} + \omega(\eta + j)/k_G|^2} \operatorname{Re}\{M_{33}^* + \omega(\eta + j)/k_G\}. \tag{9}$$

Let us now assume a random variability of the joint characteristics, and analyse its effect on the transmitted power.

In this analysis $k_G$ is a random parameter defined as

$$k_G = k_{G_0}(1 + x) \tag{10}$$

where $k_{G_0}$ is the reference deterministic stiffness and $x$ is a dimensionless random variable. For the sake of simplicity, we introduce the following quantities:

$$\mu = |M_{21} F_1|^2 \qquad \alpha = \mu \operatorname{Re}\{M_{33}^*\}, \qquad \beta = \operatorname{Re}\{M_{33}\} + \operatorname{Re}\{M_{22}\}, \tag{11}$$

$$\gamma = \operatorname{Im}\{M_{33}\} + \operatorname{Im}\{M_{22}\}, \qquad \delta = \beta^2 + \gamma^2$$

$$A = 2\left[1 + \frac{\omega(\beta\eta + \gamma)}{k_{G_0}\delta}\right], \qquad B = 1 + \frac{\omega^2}{k_{G_0}^2 \delta} + \frac{2\omega(\beta\eta + \gamma)}{k_{G_0}\delta} \tag{12}$$

so that $P_3$ and $P_2$ can be written as

$$P_3 = \frac{\alpha}{2\delta} \frac{x^2 + 2x + 1}{x^2 + Ax + B} \tag{13}$$

$$P_2 = -P_3 - \frac{\mu\eta\omega}{2k_{G_0}\delta} \frac{x + 1}{x^2 + Ax + B}. \tag{14}$$

These expressions explicitly provide the dependency of the transmitted powers on the random perturbation $x$ that is necessary for the development of the power statistics.

## 4. STATISTICS OF THE ENERGY FLOW

The statistical moments of the energy flow can be determined once the probability density function (p.d.f.) of $x$, $p(x)$, is assigned. On the basis of equations (8) and (9) mean and variance of the power can be determined as

$$E\{P_i^n(x)\} = \int_{-\infty}^{\infty} p(x)\, P_i^n(x)\, \mathrm{d}x, \qquad n = 1, 2, \quad i = 2, 3. \tag{15}$$

Although for special forms of p.d.f. it is possible to calculate mean and variance in closed form, in general this chance is denied.

In this paper, we analyse small variation of the random parameters. When $x$ is small, a series expansion of equations (13) and (14) can be performed, so that the statistical moments of the energy flow can be determined for any p.d.f. in closed form [9, 10].

Expanding equations (13) and (14) in power series up to the first order around $x = 0$, we have

$$P_i \simeq P_i|_{x=0} + \left.\frac{\partial P_i}{\partial x}\right|_{x=0} x, \quad i = 2, 3$$

provided that $\partial P_i\, \partial x|_{x=0}$ exists and it is finite (see later on).

Thus, the energy flows can be written as

$$P_3 \simeq C_{3_0} + C_{3_1} x$$
$$P_2 \simeq C_{2_0} + C_{2_1} x \tag{16}$$

where

$$C_{3_0} = \frac{\alpha}{2B\delta}, \qquad C_{3_1} = \frac{\alpha(2B - A)}{2B^2\delta}.$$
$$C_{2_0} = -\frac{k_{G_0}\alpha + \mu\eta\omega}{2k_{G_0}B\delta}, \quad C_{2_1} = \frac{k_{G_0}\alpha(A - 2B) + \eta\mu\omega(A - B)}{2k_{G_0}B^2\delta}. \tag{17}$$

Consequently the first two statistical moments of $P_2$ and $P_3$ are

$$m_{P_3} = C_{3_0}, \quad \sigma_{P_3}^2 = C_{3_1}^2\sigma_x^2$$
$$m_{P_2} = C_{2_0}, \quad \sigma_{P_2}^2 = C_{2_1}^2\sigma_x^2. \tag{18}$$

These results deserve some comments. The chance of obtaining equations (16) is related to the existence of $\partial P_i/\partial x|_{x=0}$, i.e. to the regularity of $P_i(x)$. In the following, before accepting results and conclusions derived from equation (16), a preliminary check on $C_{3_1}$ and $C_{2_1}$ is made to be sure that these functions behave sufficiently well around $x = 0$. Nevertheless, theoretical considerations on the legitimate use of equation (16) can be stressed in general (see Appendix C).

Although a first-order Taylor expansion is used, that is valid under the assumption of small perturbations, the analysis allows quite general conclusions. In fact, equations (18) are valid whatever the p.d.f. of $x$. Moreover, $\sigma_{P_3}^2$ and $\sigma_{P_2}^2$ are explicitly related to $\sigma_x^2$, i.e. to the dispersion of the joint stiffness. In this way the coefficients $C_{3_1}$ and $C_{2_1}$ play the role of amplification or attenuation factors of the joint dispersion. Since they depend on $\omega$ as indicated by equation (17), some important properties of $\sigma_{P_3}$ and $\sigma_{P_2}$, when varying the frequency, can be predicted following the analysis outlined in the next sections.

## 5. DEFINITION OF A CONFIDENCE FACTOR

To understand whether the mean may well represent the behaviour of the energy flow, a confidence factor can be defined as

$$f_c = \left| \frac{m}{\sigma} \right|. \tag{19}$$

This is the inverse of the normalised standard deviation. The confidence factor controls the width of the dispersion band around the mean value. A high value of the confidence factor corresponds to a narrow dispersion around the mean while a low value implies a large dispersion of data around the mean.

A meaningful analytical expression of the confidence factor can be found in the case of the linearised analysis previously developed. From equations (18) and (19), one has

$$f_{c_3} = \left| \frac{m_{P_3}}{\sigma_{P_3}} \right| = \left| \frac{C_{3_0}}{C_{3_1}} \right| \left| \frac{1}{\sigma_x} \right|, \qquad f_{c_2} = \left| \frac{m_{P_2}}{\sigma_{P_2}} \right| = \left| \frac{C_{2_0}}{C_{2_1}} \right| \left| \frac{1}{\sigma_x} \right|. \tag{20}$$

The confidence factors (20) are the crucial elements discussed in this paper. They provide the sought relationships between the power confidence factor and the variance of the random stiffness. Although $C_{3_0}$, $C_{3_1}$, $C_{2_0}$, $C_{2_1}$ are complicated functions of the mobilities and the system parameters, interesting conclusions can be drawn on the basis of equation (20) by performing:

- an asymptotic frequency analysis;
- a near-by resonance analysis;
- a coupling strength analysis.

The following section develops these points. Before doing this, it is convenient to rewrite equations (20) by expressing explicitly the dependence on $k_{G_0}$:

$$f_{c_3} = \left| \frac{k_{G_0}^2 \delta + 2 k_{G_0} \omega(\beta\eta + \gamma) + \omega^2}{2 k_{G_0} \omega(\beta\eta + \gamma) + 2\omega^2} \right| \left| \frac{1}{\sigma_x} \right|$$

$$f_{c_2} = \left| \frac{(k_{G_0}\alpha + \eta\mu\omega)(k_{G_0}^2 \delta + 2 k_{G_0} \omega(\beta\eta + \gamma) + \omega^2)}{k_{G_0}^2 \omega(2\alpha\beta\eta + 2\alpha\gamma - \eta\mu\delta) + 2 k_{G_0}\alpha\omega^2 + \eta\mu\omega^3} \right| \left| \frac{1}{\sigma_x} \right|. \tag{21}$$

## 6. ANALYSIS OF THE CONFIDENCE FACTOR

An asymptotic analysis can be developed to provide the limit values of $f_{c_3}$ and $f_{c_2}$ when $\omega$ tends to infinity: they provide the trend of the power data dispersion as the frequency increases.

First, an asymptotic analysis of the confidence factors in equation (21) is performed. Table 1 summarises the main results, while the calculations are reported in Appendix A. Thus, it can be proved that

$$\lim_{\omega \to \infty} f_{c_3} = \frac{1}{2} \left| \frac{1}{\sigma_x} \right|, \qquad \lim_{\omega \to \infty} f_{c_2} = \left| \frac{1}{\sigma_x} \right|. \tag{22}$$

TABLE 1

*Asymptotic trend for quantities appearing in equations (11)*

| Quantity | Re$\{M\}$ | Im$\{M\}$ | $|M|$ | $\beta$ | $\gamma$ | $\delta$ | $\alpha$ | $\mu$ |
|---|---|---|---|---|---|---|---|---|
| Tend to zero as | $1/\omega$ | $1/\omega$ | $1/\omega$ | $1/\omega$ | $1/\omega$ | $1/\omega^2$ | $1/\omega^3$ | $1/\omega^2$ |

Equations (22) provide a useful information for a complete statistical analysis of the energy flow.

It must be noticed that the difference between the two factors can be attributed to the joint's loss factor $\eta$. In fact, when $\eta$ is equal to zero both factors assume the same value $|1/2\sigma_x|$, $P_3$ being equal to $P_2$. In the case of a damped joint, $P_3$ is not equal to $P_2$ and the confidence factor of $P_2$ is larger than the one related to $P_3$.

The analysis of equations (20) reveals that $C_{3_0}$, $C_{3_1}$, $C_{2_0}$, $C_{2_1}$ depend on the mobilities of the uncoupled systems I and II. Since the mobilities have a peak in correspondence to any resonance frequency, it is suggested that the confidence factors $f_{c_3}$ and $f_{c_2}$ present critical values in correspondence to any of the resonance frequencies $\omega_{n_I}$ and $\omega_{n_{II}}$ of I and II, respectively. If the dampings of I and II are not too high, very large values of $M_{ij}$ are expected when $\omega$ tends to $\omega_n$. Since the analysis is performed in a frequency range close to the studied eigenfrequencies, the contribution of the other modes of a multi-degree-of-freedom system can be neglected at least when the modal overlap is sufficiently low. By putting $\epsilon_I = \omega^2 - \omega_{n_I}^2$ and $\epsilon_{II} = \omega^2 - \omega_{n_{II}}^2$, the behaviour of the terms appearing in equation (21) are summarised in Tables 2 and 3 for $\omega^2 \to \omega_{n_I}^2$ and $\omega^2 \to \omega_{n_{II}}^2$, respectively. By these results it follows that $f_{c_3}(\omega_n)$ tends to infinity for any natural frequency $\omega_n$ of I and II. On the contrary, the confidence factor $f_{c_2}(\omega_n)$ tends to infinity for any natural frequency $\omega_n$ of II, while, in correspondence of the natural frequencies of I, a finite value of $f_{c_2}$ is obtained.

The presence of the mentioned critical points provides, close to the resonance of either I or II, a large amplification of the confidence factors of the power flow, i.e. the dispersion on the results is low. This effect, on the basis of the developed asymptotic analysis, tends to be cancelled when the frequency increases, leading to the 'stationary' (non-oscillatory) trend expressed by equations (22).

Therefore, there are two different frequency regions where the confidence factors present different behaviours: the first one is rather oscillatory, while the second one is almost uniform. These two different trends are related to the value of $k_{G_0}$. Considering equations (21), it is apparent that, when both the following conditions hold for $f_{c_3}$:

$$\omega^2 \gg k_{G_0}^2 \delta + 2k_{G_0}\omega(\beta\eta + \gamma)$$
$$2\omega^2 \gg 2k_{G_0}\omega(\beta\eta + \gamma) \tag{23}$$

TABLE 2

*Behaviour of quantities appearing in equations (11) for $\omega^2 \to \omega_{n_I}^2$, i.e. $\epsilon_I \to 0$*

| Quantity | $\beta$ | $\gamma$ | $\delta$ | $\mu$ | $\alpha$ |
|---|---|---|---|---|---|
| Tends to | $1/\epsilon_I^2$ | $\epsilon_I$ | $1/\epsilon_I^4$ | $1/\epsilon_I^4$ | $1/\epsilon_I^4$ |

TABLE 3

*Behaviour of quantities appearing in equations (11) for $\omega^2 \to \omega_{n_{II}}^2$, i.e. $\epsilon_{II} \to 0$*

| Quantity | $\beta$ | $\gamma$ | $\delta$ | $\mu$ | $\alpha$ |
|---|---|---|---|---|---|
| Tends to | $1/\epsilon_{II}^2$ | $\epsilon_{II}$ | $1/\epsilon_{II}^4$ | Finite value | $1/\epsilon_{II}^2$ |

and for $f_{c_2}$

$$\eta\mu\omega^3 \gg (k_{G_0}\alpha + \eta\mu\omega)\left[k_{G_0}^2\delta + 2k_{G_0}\omega(\beta\eta + \gamma)\right] + k_{G_0}\alpha\omega^2$$

$$\eta\mu\omega^3 \gg 2k_{G0}\alpha\omega^2 + k_{G_0}^2\omega(2\alpha\beta\eta + 2\alpha\gamma - \eta\mu\delta) \tag{24}$$

then we obtain

$$f_{c_3} \simeq \left|\frac{\omega^2}{2\omega^2}\right|\left|\frac{1}{\sigma_x}\right| = \frac{1}{2}\left|\frac{1}{\sigma_x}\right|$$

and

$$f_{c_2} \simeq \left|\frac{\eta\mu\omega^3}{\eta\mu\omega^3}\right|\left|\frac{1}{\sigma_x}\right| = \left|\frac{1}{\sigma_x}\right|.$$

As we can see the confidence factors tend to become constant and equal to the asymptotic value given in equation (22).

The conditions (23) and (24) help in defining the two frequency ranges separating the oscillatory from the non-oscillatory regions. In order to estimate these values, a non-dimensional mobility expression is required.

Choosing the non-dimensional form for the eigenfrequencies, $\tilde{\omega}_n = \omega_n/\omega$, the mobility of a modal system can be written as follows:

$$M_{ij} = \frac{\chi}{m_T\omega}\sum_n \frac{\varphi_n(\zeta_i)\varphi_n(\zeta_j)}{\tilde{\omega}_n^2\eta + j(1 - \tilde{\omega}_n^2)}$$

where $\varphi$ is the eigenfunction, $m_T$ is the mass of the system and $\chi$ is a constant: its value is $\chi = 2$ for one-dimensional structures (beams) and $\chi = 4$ for two-dimensional structures (plates). Equation (11) can be rewritten in a non-dimensional way as

$$\tilde{\beta} = \frac{m_T\omega}{\chi}\beta, \quad \tilde{\gamma} = \frac{m_T\omega}{\chi}\gamma, \quad \tilde{\delta} = \frac{m_T\omega}{\chi}\delta \tag{25}$$

so that equations (23) and (24) become

$$\omega^2 \gg \frac{\chi^2 k_{G_0}}{m_T}\left(\frac{k_{G_0}}{m_T\omega^2}\tilde{\delta} + \tilde{\beta}\eta + \tilde{\gamma}\right)$$

$$2\omega^2 \gg \frac{\chi^2 k_{G_0}}{m_T}(\tilde{\beta}\eta + \tilde{\gamma}) \tag{26}$$

and

$$\eta\omega^3 \gg (k_{G_0}\frac{\chi}{m_T\omega}\mathrm{Re}\{\tilde{M}_{33}\} + \eta\omega)\left[k_{G_0}^2\frac{\chi^2}{m_T^2\omega^2}\tilde{\delta} + 2k_{G_0}\omega\frac{\chi}{m_T\omega}(\tilde{\beta}\eta + \tilde{\gamma})\right]$$

$$+ k_{G_0}\omega^2\frac{\chi}{m_T\omega}\mathrm{Re}\{\tilde{M}_{33}\} \tag{27}$$

$$\eta\omega^3 \gg 2k_{G_0}\omega^2\frac{\chi}{m_T\omega}\mathrm{Re}\{\tilde{M}_{33}\} + k_{G_0}^2\omega\frac{\chi^2}{m_T^2\omega^2}\left(2\tilde{\beta}\eta\mathrm{Re}\{\tilde{M}_{33}\} + 2\tilde{\gamma} - \eta\tilde{\delta}\right).$$

Since the mobility has a peak at resonance, it is possible to maximise the non-dimensional quantities. At resonance, $\tilde{\omega}$ is equal to unity and the value of the eigenvector product, $\varphi_n(x_i)\varphi_n(x_j)$ can be maximised by substituting the unit value; therefore, the maxima of the non-dimensional quantities are

$$\tilde{M} \simeq \frac{1}{\eta}, \quad \mathrm{Re}\{\tilde{M}\} \simeq \frac{1}{\eta}, \quad \mathrm{Im}\{\tilde{M}\} \simeq 0, \quad \tilde{\beta} \simeq \frac{2}{\eta}, \quad \tilde{\gamma} \simeq 0, \quad \tilde{\delta} \simeq \frac{4}{\eta^2}. \tag{28}$$

Substituting equation (28) into equations (26) and (27), one has

$$\omega^4 - \frac{2\chi^2 k_{G_0}}{m_T}\omega^2 - \frac{4\chi^2 k_{G_0}^2}{m_T^2 \eta^2} \gg 0$$

$$\omega^2 \gg \frac{\chi^2 k_{G_0}}{m_T} \tag{29}$$

and

$$\eta\omega^6 - \left(\frac{4k_{G_0}\chi}{m_T} + \frac{k_{G_0}\chi}{m_T\eta}\right)\omega^4 - \frac{8k_{G_0}^2\chi^2}{m_T^2\eta}\omega^2 - \frac{4k_{G_0}^3\chi^3}{m_T^3\eta^3} \gg 0$$

$$\eta\omega^4 - \frac{2k_{G_0}\chi}{m_T\eta}\omega^2 \gg 0. \tag{30}$$

Since $\eta \ll 1$, the first equation in equation (29) has the following two solutions:

$$\omega^2 = \pm\frac{2\chi k_{G0}}{m_T\eta}$$

but the second one restricts the frequency range of the asymptotic (non-oscillatory) behaviour of $f_{c_3}$ to the following value:

$$\omega^2 \gg \frac{2\chi k_{G_0}}{m_T\eta} \tag{31}$$

For the second equation (30), the following condition can be written:

$$\omega^2 \gg \frac{2\chi k_{G0}}{m_T\eta^2} \tag{32}$$

while the first equation (30), with $\eta \ll 1$, becomes

$$\left(\omega^2\right)^3 - \frac{k_{G_0}\chi}{m_T\eta^2}\left(\omega^2\right)^2 - \frac{8k_{G_0}^2\chi^2}{m_T^2\eta^2}\omega^2 - \frac{4k_{G_0}^3\chi^3}{m_T^3\eta^6} \gg 0 \tag{33}$$

whose solution yields

$$\omega^2 \gg \frac{\chi k_{G_0}}{2m_T\eta^2}. \tag{34}$$

Comparing equation (34) with equation (32) it is obvious that the last condition can provide a reference frequency separating the oscillatory and non-oscillatory regions of the confidence factor $f_{c_2}$. Moreover, this transition frequency has a lower value for $f_{c_3}$.

## 7. ANALYSIS OF OTHER RESONANT AND NON-RESONANT SYSTEMS

In this section, the other three dynamic systems indicated in Section 2 are briefly described and the behaviour of their confidence factors is presented. Calculations are developed in detail in Appendix B.

7.1. WAVE GUIDE WITH RANDOM YOUNG MODULUS

The longitudinal wave field displacement of the uniform infinite rod, shown in Fig. 2, is given by

$$w(\zeta, t) = We^{j(\omega t - k\zeta)}. \tag{35}$$

The longitudinal force in the rod is given by

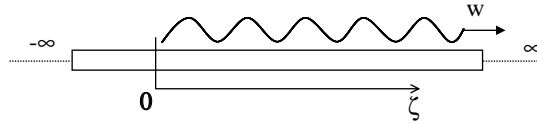$$N(\zeta, t) = ES\frac{\partial w}{\partial \zeta} \tag{36}$$

Figure 2. The wave guide.

S being the cross-sectional area of the rod. The energy flow at abscissa $\zeta = \bar{\zeta}$ is determined by

$$P = \frac{1}{2}\operatorname{Re}\{N\dot{w}^*\}|_{\zeta=\bar{\zeta}} \tag{37}$$

that, by the equations (35) and (36), becomes

$$P = -\frac{1}{2}S\omega^2\sqrt{\rho E}|W|^2. \tag{38}$$

It is assumed that Young's modulus of the rod is random, i.e. $E = E_0(1 + x)$, $E_0$ being the reference value, and $x$ a non-dimensional random variable. By a perturbation technique, mean, standard deviation and confidence factor of the power flow are calculated. In particular for $f_c$ we have

$$f_c = \left|\frac{P|_{x=0}}{\partial P/\partial E|_{x=0}E_0}\right|\left|\frac{1}{\sigma_x}\right|. \tag{39}$$

By substituting equation (38) into equation (39), the confidence factor appears to be a constant function not depending on frequency, i.e.

$$f_c = 2\left|\frac{1}{\sigma_x}\right|. \tag{40}$$

### 7.2. RESONATOR WITH RANDOM YOUNG MODULUS

The system considered is a finite continuous system exited at an arbitrary point by a force $F_1$. Its Young's modulus is a random variable, $E = E_0(1 + x)$ and the system mobility has the general expression

$$M_{qr} = \omega\Theta\sum_n\frac{\varphi_n(\zeta_q)\varphi_n(\zeta_r)}{\omega_n^2\eta + j(\omega^2 - \omega_n^2)} \tag{41}$$

$\Theta$ being a coefficient depending on the system parameters. The energy flow is

$$P = \frac{1}{2}|F|^2\operatorname{Re}\{M^*\} \tag{42}$$

and the confidence factor is evaluated by a perturbation technique to yield

$$f_c = \left|\frac{\operatorname{Re}\{M\}|_{x=0}}{\partial\operatorname{Re}\{M\}/\partial\omega_n\,\partial\omega_n/\partial E|_{x=0}E_0}\right|\left|\frac{1}{\sigma_x}\right|. \tag{43}$$

In this case, the system being modal, the confidence factor is frequency dependent, but the asymptotic analysis shows that $f_c$ tends to a constant value, given by

$$\lim_{\omega\to\infty}f_c = \left|\frac{1}{\sigma_x}\right|. \tag{44}$$
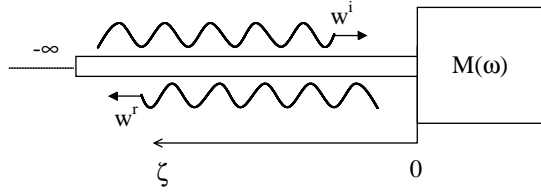
Figure 3. Wave guide with random Young's modulus coupled with a resonator.

### 7.3. WAVE GUIDE WITH RANDOM YOUNG MODULUS COUPLED WITH A RESONATOR

Fig. 3 shows a semi-infinite rod connected with a resonator. The wave field on the guide consists of a pair of waves, incident and reflected, i.e. expressed by

$$w^i = W^i e^{j(\omega t - k\zeta)}, \quad w^r = W^r e^{j(\omega t + k\zeta)}. \tag{45}$$

The total displacement field is $w = w^i + w^r$, and the complex reflection coefficient is defined as: $r = W^r / W^i$.

The forces $N$ in the wave guide are given by:

$$N^i = ES\frac{\partial w^i}{\partial \zeta}, \quad N^r = ES\frac{\partial w^r}{\partial \zeta}, \quad N = N^i + N^r \tag{46}$$

and the energy flow at the origin of the reference frame is

$$P = \frac{1}{2}\mathrm{Re}\{N\dot{w}^*\}|_{\zeta=0} = \frac{1}{2}S\sqrt{E\rho}\,\omega^2|W^i|^2(1 - |r|^2). \tag{47}$$

$f_c$ is computed again by a perturbation technique. In Appendix B the full development is presented. The confidence factor is frequency dependent, because a resonator is included in the system. The behaviour of the mobility for $\omega \to \infty$ is reported in Table 1. Thus, it can be proved that

$$\lim_{\omega \to \infty} f_c = \left|\frac{1}{\sigma_x}\right|. \tag{48}$$

### 7.4. WAVE GUIDE–JOINT WITH RANDOM STIFFNESS–WAVE GUIDE

Two equal semi-infinite, uniform, rods are connected as shown in Fig. 4. The joint has a random stiffness: $k_G = k_{G_0}(1 + x)$. An incoming incident wave $w_1^i$ propagates along rod 1 towards the origin. A reflected wave $w_1^r$ is generated in rod 1 at the joint location ($\zeta_1 = 0$) and a wave $w_2^t$ is transmitted along rod 2. With the reference frame of Fig. 4, the three waves can be expressed by

$$w_1^i = W_1^i e^{j(\omega t + k_1\zeta_1)}, \quad w_1^r = W_1^r e^{j(\omega t - k_1\zeta_1)} \quad w_2^t = W_2^t e^{j(\omega t - k_2\zeta_2)}. \tag{49}$$

The reflection and the transmission coefficients are, respectively:

$$r = \frac{W_1^r}{W_1^i}, \quad \tau = \frac{W_2^t}{W_1^i}. \tag{50}$$

Their values are calculated from the equilibrium conditions:

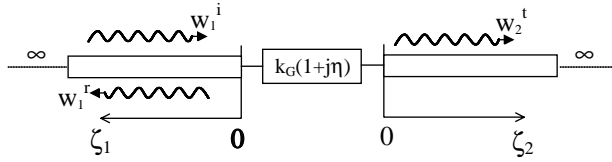$$N_1|_{\zeta_1=0} = N_2|_{\zeta_2=0}, \quad k(1 + j\eta)(w_1 + w_2)|_{\zeta_{1,2}=0} = -N_2|_{\zeta_2=0} \tag{51}$$

Figure 4. Wave guide–random joint–wave guide.

so that one has, for the above coefficients

$$r = \frac{[k_G(1 + \varsigma) - \omega v \eta]^2 + \omega^2 v^2 - 2\varsigma k_G[k_G(1 + \varsigma) - \omega v \eta] + j2k_G \omega \varsigma v}{[k_G(1 + \varsigma) - \omega v \eta]^2 + \omega^2 v^2} \tag{52}$$

$$\tau = -\frac{2k_G[k_G(1 + \varsigma) - \omega v \eta] + j2k\omega v}{[k_G(1 + \varsigma) - \omega v \eta]^2 + \omega^2 v^2} \tag{53}$$

where the coefficient $\varsigma$, $v$ and $\psi$ are, respectively:

$$\varsigma = \frac{S_2\sqrt{E_2\rho_2}}{S_1\sqrt{E_1\rho_1}}, \quad v = \frac{S_2\sqrt{E_2\rho_2}}{1 + \eta^2}, \quad \psi = v(\eta + j). \tag{54}$$

The energy flows calculated at $\zeta_1 = 0$ and $\zeta_2 = 0$ are, respectively:

$$P_1 = \frac{1}{2}\operatorname{Re}\{N_1\dot{w}_1^*\}\big|_{\zeta_1 = 0} = \frac{1}{2}\omega^2 S_1\sqrt{E_1\rho_1}\left|W_1^i\right|^2\left(1 - |r|^2\right) \tag{55}$$

$$P_2 = \frac{1}{2}\operatorname{Re}\{N_2\dot{w}_2^*\}\big|_{\zeta_2 = 0} = \frac{1}{2}\omega^2 S_2\sqrt{E_2\rho_2}\left|W_2^i\right|^2|\tau|^2. \tag{56}$$

Finally, the confidence factors obtained by the perturbation technique, are:

$$f_{c_1} = \left|\frac{P_1|_{x=0}}{\partial P_1/\partial k_G|_{x=0}k_{G_0}}\right|\left|\frac{1}{\sigma_x}\right|, \quad f_{c_2} = \left|\frac{P_2|_{x=0}}{\partial P_2/\partial k_G|_{x=0}k_{G_0}}\right|\left|\frac{1}{\sigma_x}\right|. \tag{57}$$

A mathematical manipulation of the confidence factors shows that $f_{c_2}$ decays monotonically with the frequency, until it reaches the constant value

$$f_{c_2} = \frac{1}{2}\left|\frac{1}{\sigma_x}\right|. \tag{58}$$

The confidence factor $f_{c_1}$ depends on the frequency like a singular-modal resonator, because two waves, incident and reflected, propagate along rod 1 and interfere. The asymptotic value reached by $f_{c_1}$ is given by

$$\lim_{\omega \to \infty} f_{c_1} = \left|\frac{1}{\sigma_x}\right|. \tag{59}$$

Table 4 summarises the obtained asymptotic behaviours of the confidence factors.

## 8. NUMERICAL RESULTS

In this section, numerical results obtained by a Monte-Carlo simulation are performed to validate the theoretical results.

Let us examine three numerical examples related to two coupled resonators. The study of these systems is interesting because it shows the trend of the confidence factor for three systems with different modal density functions.

TABLE 4

*Confidence factors for $\omega \to \infty$*

|  | Constant value | Asymptotic value |
|---|---|---|
| Random w. g. | $f_c = \lvert 2/\sigma_x \rvert$ | |
| Random r. | | $f_c \to \lvert 1/\sigma_x \rvert$ |
| Random w. g.–r. | | $f_c \to \lvert 1/\sigma_x \rvert$ |
| w. g.–random j.–w. g. | | $f_{c_1} \to \lvert 1/\sigma_x \rvert \quad f_{c_2} \to \lvert 1/(2\sigma_x) \rvert$ |

The first system consists of two coupled beams: bending waves are considered, where the modal density varies as $1/\sqrt{\omega}$.

The second system analysed consists of two coupled plates. Also in this case bending waves are studied. The modal density is independent of frequency.

The third system is a cylindrical thin shell coupled with a transversely flexural plate. An analytical expression for the modal density of this mechanical system does not exist, but it is possible to use, as an approximate value, the modal density of a thin pipe. This increases as $\sqrt{\omega}$ until a particular frequency, given by the following equation, is reached [2]:

$$\omega = \frac{1}{R}\sqrt{\frac{E}{\rho(1 - v^2)}}.$$

Beyond this frequency the modal density is constant.

These three systems have a joint random stiffness defined by equation (10). A Gaussian probability density function is chosen for the random variable $x$, with zero mean and standard deviation $\sigma_x = 0.05$.

8.1. BEAM–JOINT WITH RANDOM STIFFNESS–BEAM SYSTEM

Two transversely vibrating supported beams are coupled together through a non-conservative joint as described in Fig. 5. The mobilities appearing in equations (6) and (7) are given by

$$M_{12} = \frac{2\omega}{\rho_I S_I L_I} \sum_n \frac{\varphi_{In}(\zeta_1)\varphi_{In}(\zeta_2)}{\eta_I \omega_{In}^2 + j(\omega^2 - \omega_{In}^2)}$$

$$M_{22} = \frac{2\omega}{\rho_I S_I L_I} \sum_n \frac{\varphi_{In}(\zeta_2)^2}{\eta_I \omega_{In}^2 + j(\omega^2 - \omega_{In}^2)}$$

$$M_{33} = \frac{2\omega}{\rho_{II} S_{II} L_{II}} \sum_n \frac{\varphi_{IIn}(\xi_3)^2}{\eta_{II} \omega_{IIn}^2 + j(\omega^2 - \omega_{IIn}^2)}. \tag{60}$$

Subscripts I and II denote the first and second beam, respectively. The expressions of the eigenfunctions, wavenumbers and natural frequencies are, respectively:

$$\varphi_n = \sin\left(\frac{n\pi\zeta}{L}\right), \quad k_n = \frac{n\pi}{L}, \quad \omega_n = k_n^2 \sqrt{\frac{E\mathscr{I}}{\rho A}} \tag{61}$$

where $\mathscr{I}$ is the section second moment of area and $S$ is the area of the cross-section.

The values of the physical parameters of the system are reported in Table 5.

The first beam is excited by a harmonic point force acting at $\zeta_1 = 0.3$ m and its amplitude is $F_1 = 1$ N. The joint is connected between the point of the first beam at $\zeta_2 = 0.7$ m and the point of the second beam at $\xi_3 = 0.4$ m.
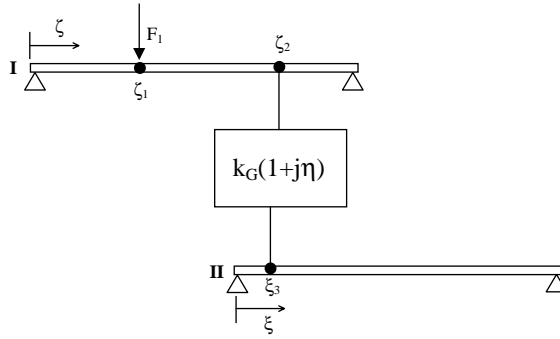
Figure 5. Two coupled beams.

*Physical parameters of the two beams*

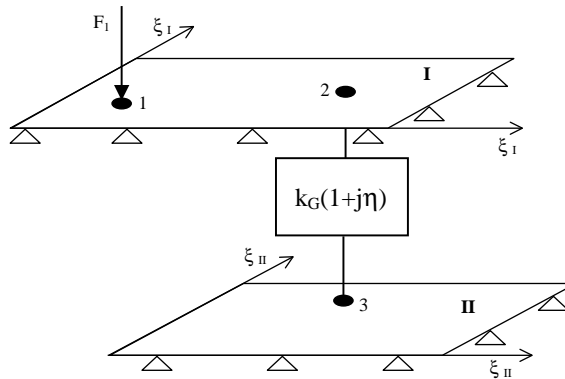|  | $E$ (Pa) | $\rho$ (kg m$^3$) | $h$ (m) | $L$ (m) | I (m$^4$) | $\eta$ |
|---|---|---|---|---|---|---|
| First beam | $2.1 \times 10^{11}$ | 7800 | 0.01 | 1.5 | $8.3 \times 10^{-10}$ | 0.01 |
| Second beam | $2.1 \times 10^{11}$ | 7800 | 0.005 | 2.5 | $5.2 \times 10^{-11}$ | 0.01 |



Figure 6. Two coupled plates

The analysis presented here is aimed to verify the theoretical conclusions drawn in Section 5. In particular, Monte-Carlo numerical simulations are performed to emphasise the behaviour of the confidence factor at high frequencies under different strength coupling conditions, and close to resonance.

Simulations corresponding to two values of $k_{G_0}$ are considered, that are representative of two different strength conditions. The first value, 1000 N/m, is an order of magnitude less than the static stiffness of the beams, while the second, 10 000 N/m, has the same order of magnitude.

In Fig. 8, the case of low strength coupling, 1000 N/m, is shown. The confidence factor $f_{c_2}$ of the two power flows, obtained by using the analytical expressions given in equations
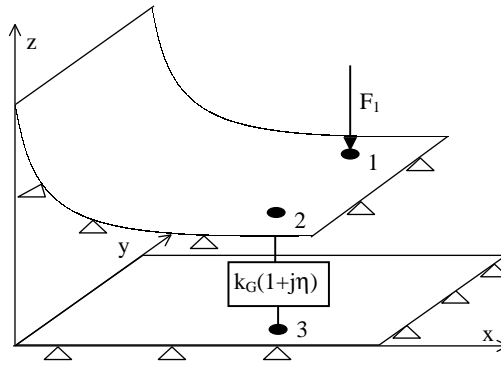
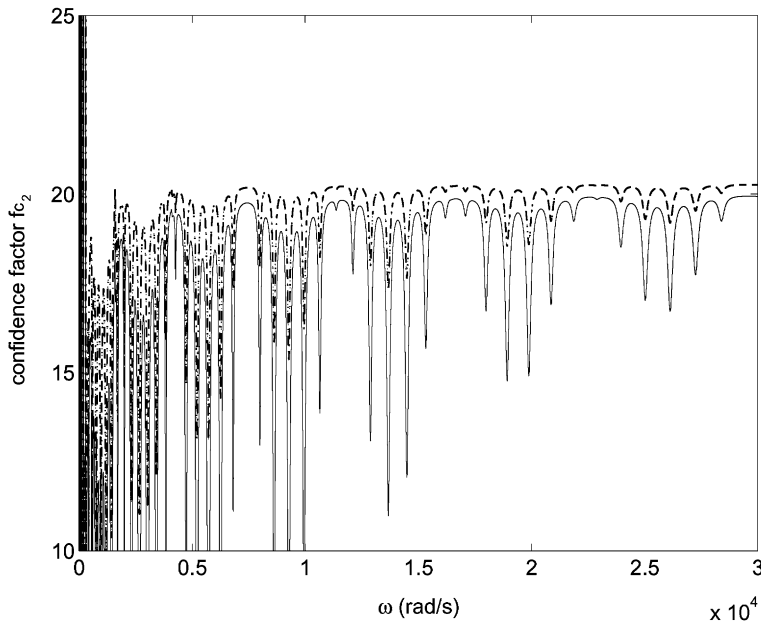Figure 7. Plate coupled with a sector—90°—of a cylindrical shell.



Figure 8. Confidence factor $f_{c_2}$ of the beam–joint with random stiffness–beam system, $k_{G_0} = 1000 \, \text{N/m}$; ——, analytical solution; -.-.-.-.-., Monte-Carlo solution.

(21) and a Monte-Carlo simulation, is plotted *vs* circular frequency. Two different trends of the confidence factors are observed: in the frequency range 0–15 000 quite strong oscillations of the curves appear, while, beyond this range, a stabilisation of $f_{c_2}$ occurs, i.e. the asymptotic behaviour is reached as predicted by equations (25), i.e.: $|1/\sigma_x| = 20$.

Fig. 9 shows the confidence factor $f_{c_3}$. Also in this figure the analytical expression and the Monte-Carlo simulation are plotted for $k_{G_0} = 1000 \, \text{N/m}$. In this case the non-oscillatory trend starts from 1000 rad/s and the asymptotic behaviour predicted by equations (25) is reached: $|1/(2\sigma_x)| = 10$.

A more accurate analysis of the curves in the range 0–350 Hz of the oscillations presented in Figs 10 and 11, shows that the peaks are located in correspondence with the
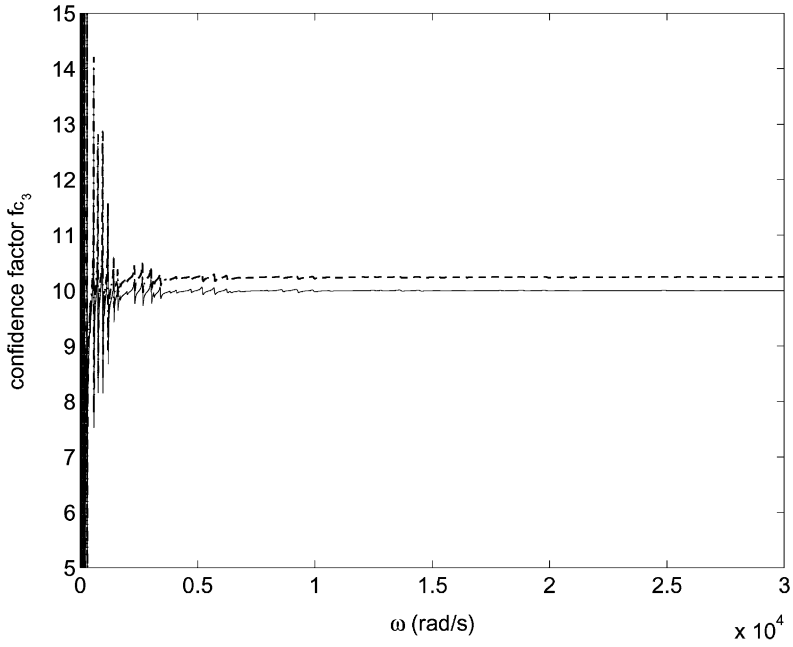
Figure 9. Confidence factor $f_{c_3}$ of the beam–joint with random stiffness–beam system, $k_{G_0} = 1000\,\text{N/m}$; ——— analytical solution; -.-.-.-.-., Monte-Carlo solution.
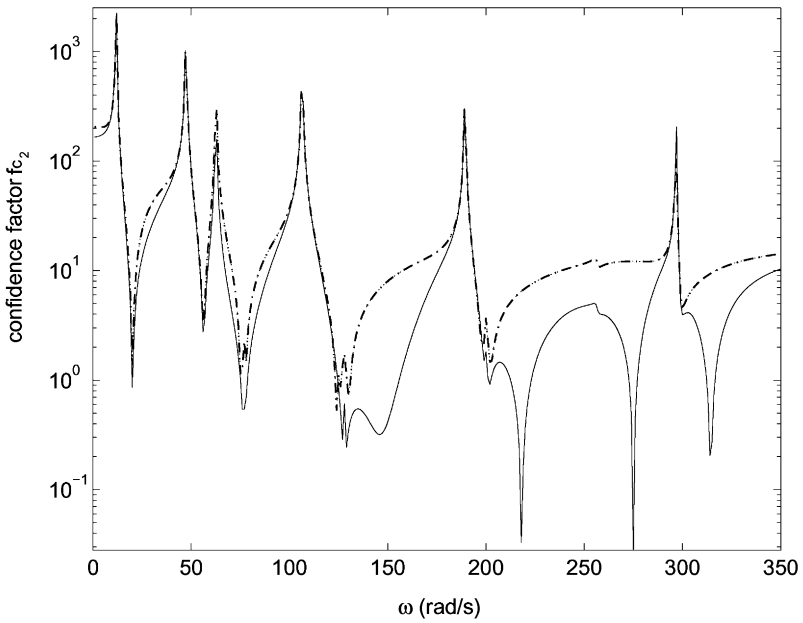


Figure 10. Confidence factor $f_{c_2}$ of the beam–joint with random stiffness–beam system, $k_{G_0} = 1000\,\text{N/m}$; ——— analytical solution; -.-.-.-.-., Monte-Carlo solution.
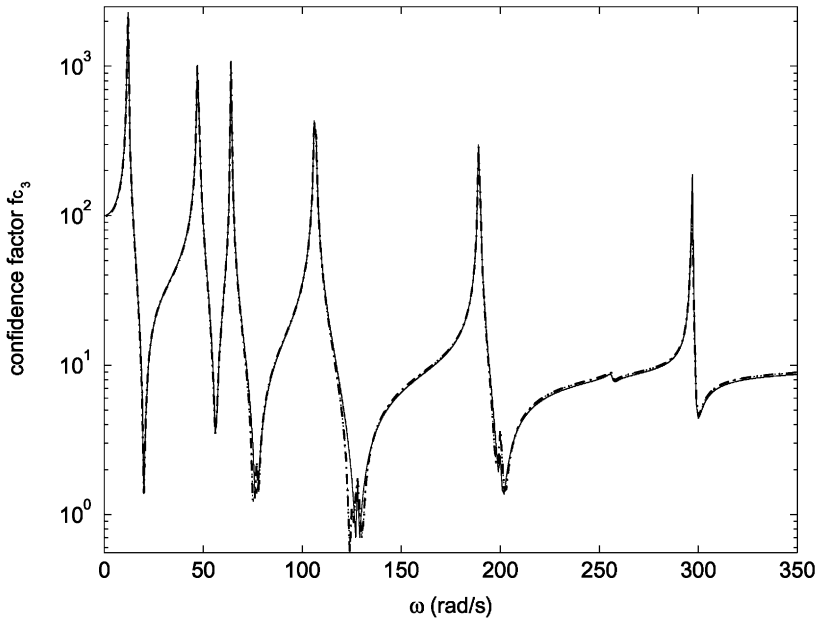
Figure 11. Confidence factor $f_{c_3}$ of the beam–joint with random stiffness–beam system, $k_{G_0} = 1000\,\text{N/m}$; ——— analytical solution; -.-.-.-.-., Monte-Carlo solution.

TABLE 6

*First six natural frequencies of the two beams*

|  | $\omega_1$ | $\omega_2$ | $\omega_3$ | $\omega_4$ | $\omega_5$ | $\omega_6$ |
|---|---|---|---|---|---|---|
| First beam | 65 | 262 | 589 | 1048 | 1637 | 2358 |
| Second beam | 12 | 47 | 106 | 189 | 295 | 425 |

natural frequencies of the two subsystem I and II. The first six natural frequencies of the two subsystems are listed in Table 6.

In Fig. 12 and 13 the confidence factors $f_{c_2}$ and $f_{c_3}$, are plotted following the pattern of Figs 8 and 9. The reference stiffness is equal to $10\,000\,\text{N/m}$. The curves of Fig. 12 show a decrease of the amplitude of oscillation, but in the frequency range examined no asymptotic behaviour is observed. The confidence factor $f_{c_3}$ plotted in Figure 13 shows an asymptotic trend beyond $4000\,\text{rad/s}$ and the value predicted in equation (25) is reached: $\left|1/(2\sigma_x)\right| = 10$.

An asymptotic value is reached also in the Monte-Carlo approach, although it differs slightly from the value predicted by the theoretical analysis. This difference can be explained by the use of a finite number of realizations in the Monte-Carlo method (200 realizations). The transition frequencies between the oscillatory and the non-oscillatory frequency region can be calculated by the conditions (31) and (32). Table 7 shows the values of the transition frequencies for both values of $k_{G_0}$.

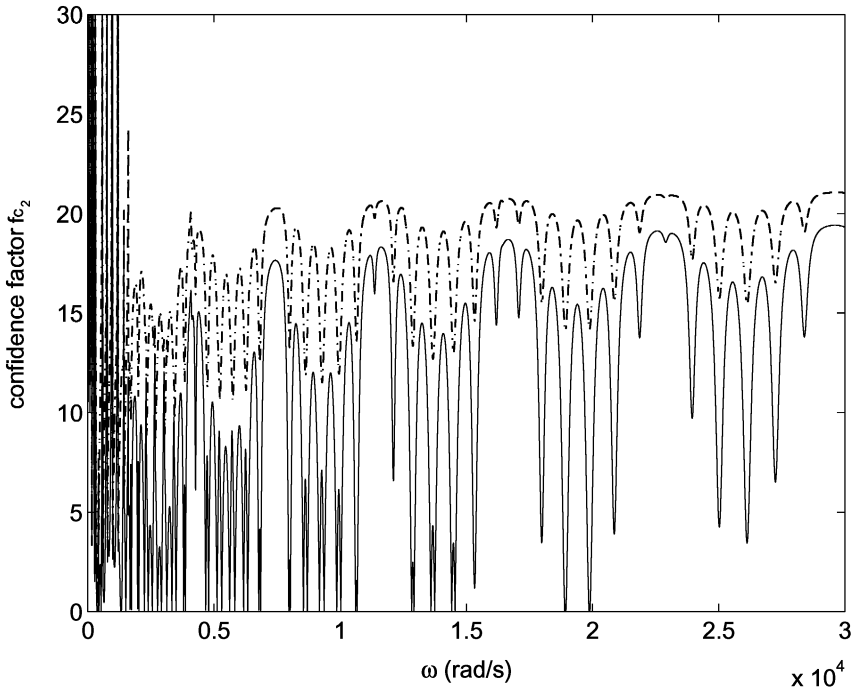The confidence factors plotted in Figs 8, 9, 12 and 13 agree sufficiently well with the results shown in Table 7.

Figure 12. Confidence factor $f_{c_2}$ of the beam–joint with random stiffness–beam system, $k_{G_0} = 10\,000\,\text{N/m}$: —— analytical solution, -.-.-.-.-., Monte-Carlo solution.
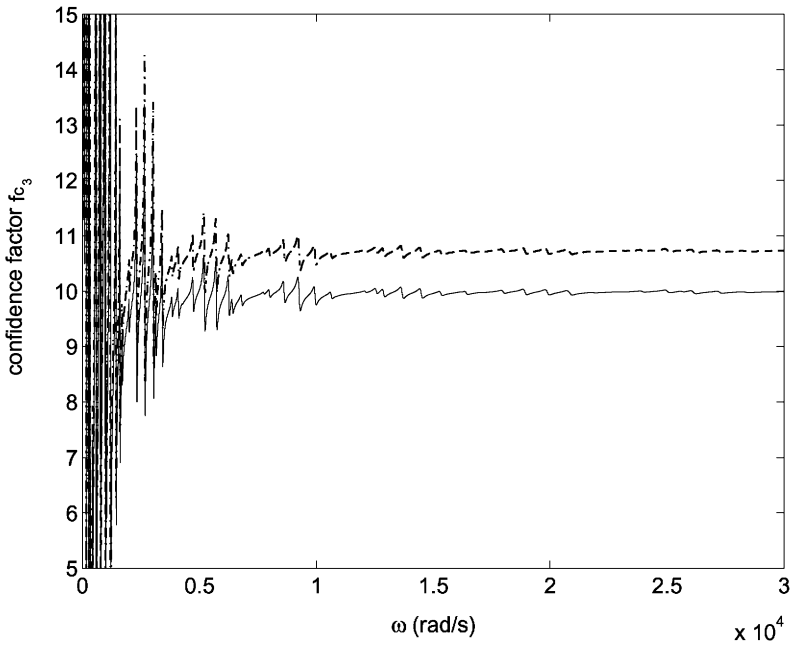


Figure 13. Confidence factor $f_{c_3}$ of the beam–joint with random stiffness–beam system, $k_{G_0} = 10\,000\text{N/m}$: —— analytical solution; -.-.-.-.-., Monte-Carlo solution.

TABLE 7

*Onset of asymptotic trend for two coupled beams*

|  | $k_{G_0} = 1000\,\text{N/m}$ | $k_{G_0} = 10\,000\,\text{N/m}$ |
|---|---|---|
| For $f_{c_2}$ | $\omega > 5000$ | $\omega > 16000$ |
| For $f_{c_3}$ | $\omega > 500$ | $\omega > 1600$ |

It is clear that in the first case the asymptotic (non-oscillatory) behaviour is reached faster than in the second case. Moreover, the amplitude of oscillations of the confidence factors are larger in the second case. This confirms the theoretical prediction stated in Section 5.

### 8.2. PLATE–JOINT WITH RANDOM STIFFNESS–PLATE SYSTEM

The second case analysed consists of two bending rectangular plates simply supported along the four edges and coupled together through a non-conservative joint (Fig. 6). Mobilities are determined as

$$M_{12} = \frac{4\omega}{\rho_\mathrm{I} h_\mathrm{I} S_\mathrm{I}} \sum_{n,m} \frac{\varphi_{Inm}(\zeta_1, \xi_1)\varphi_{In}(\zeta_2, \xi_2)}{\eta_\mathrm{I}\omega_{Inm}^2 + j(\omega^2 - \omega_{Inm}^2)}$$

$$M_{22} = \frac{4\omega}{\rho_\mathrm{I} h_\mathrm{I} S_\mathrm{I}} \sum_{n,m} \frac{\varphi_{Inm}(\zeta_2, \xi_2)^2}{\eta_\mathrm{I}\omega_{Inm}^2 + j(\omega^2 - \omega_{Inm}^2)}$$

$$M_{33} = \frac{4\omega}{\rho_\mathrm{II} h_\mathrm{II} S_\mathrm{II}} \sum_{n,m} \frac{\varphi_{IInm}(\zeta_3, \xi_3)^2}{\eta_\mathrm{II}\omega_{IInm}^2 + j(\omega^2 - \omega_{IInm}^2)}. \tag{62}$$

$S_\mathrm{I}$ and $S_\mathrm{II}$, $h_\mathrm{I}$ and $h_\mathrm{II}$ are the plate surface areas, and the thickness of each plate, respectively. The mode shapes, wavenumbers and natural frequencies are given by

$$\varphi_{nm} = \sin\left(\frac{n\pi\zeta}{L_\zeta}\right)\sin\left(\frac{n\pi\zeta}{L_\xi}\right), \quad k_{nm} = \sqrt{\left(\frac{n\pi}{L_\zeta}\right)^2 + \left(\frac{m\pi}{L_\xi}\right)^2} \tag{63}$$

$$\omega_{nm} = k_{nm}^2 \sqrt{\frac{Eh^2}{12\rho(1-v^2)}}.$$

The first plate is excited by a harmonic force acting at ($\zeta_1 = 0.1$ and $0.15\,\text{m}$) and its amplitude is $F_1 = 1\,\text{N}$. The joint connects the point ($\zeta_2 = 0.45$ and $0.3\,\text{m}$) of the first plate with the point ($\zeta_3 = 0.23$ and $0.34\,\text{m}$) of the second plate. The physical parameters of the system are given in Table 8.

As in the previous case, two different values of the reference stiffness are used to account for different coupling conditions: $k_{G_0} = 1000\,\text{N/m}$ and $k_{G_0} = 10\,000\,\text{N/m}$. Figures 14 and 15 show the confidence factors $f_{c_2}$ and $f_{c_3}$, for $k_{G_0} = 1000\,\text{N/m}$. By analysing these figures one can observe (Fig. 14) that the asymptotic value, $f_{c_2} = 20$, is reached beyond 10 000 rad/s while $f_{c_3}$ assumes the asymptotic value 10 beyond 1000 rad/s, as predicted by the theoretical expressions (Fig. 15).

Figures 16 and 17 show the confidence factors for $k_{G_0} = 10\,000\,\text{N/m}$. The confidence factor $f_{c_2}$ shows a decrease of the oscillation amplitudes and it tends to the predicted asymptotic value 20. The confidence factor $f_{c_3}$ reaches the asymptotic value 10 beyond 3000 rad/s.

TABLE 8

*Physical parameters of the two plates*

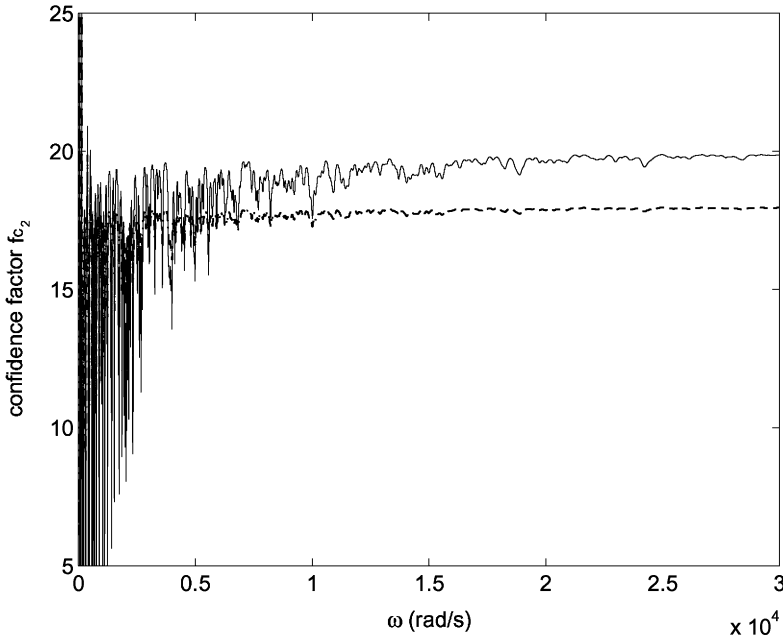|              | $E$ (Pa)             | $\rho$ (kg m$^3$) | $v$  | $h$ (m) | $L_\zeta$ (m) | $L_\xi$ (m) | $\eta$ |
|--------------|---------------------|-------------------|------|---------|---------------|-------------|--------|
| First plate  | $2.1 \times 10^{11}$ | 7800              | 0.28 | 0.002   | 1.0           | 1.0         | 0.01   |
| Second plate | $2.1 \times 10^{11}$ | 7800              | 0.28 | 0.0025  | 1.5           | 1.0         | 0.01   |



Figure 14. Confidence factor $f_{c_2}$ of the plate–joint with random stiffness–plate system, $k_{G_0} = 1000$ N/m: ——, analytical solution; -.-.-.-.-., Monte-Carlo solution.

In Table 9 the values of the transition frequencies calculated by equations (31) and (32) are reported. The results obtained by the Monte-Carlo simulation agree sufficiently well with those of Table 9 and with the theoretical statement of Section 5.

8.3. SHELL–JOINT WITH RANDOM STIFFNESS–PLATE SYSTEM

In a third numerical case the coupling of two two-dimensional structures is considered.

Figure 7 shows the model: a sector—90°—of a cylindrical shell is connected to a plate by a hysteretic-elastic joint. In Table 10 the values of the physical parameters are reported. The shell and the plate are simply supported along all the sides. The shell is forced at point 1 ($x = 0.55$ m, $y = 1$ m, $z = 0.11$ m) with a harmonic force, $F_1$, directed along the $z$-axis and amplitude 1 N. The joint connects point 2 ($x = 0.55$ m, $y = 0.2$ m, $z = 0.11$ m) of the shell and point 3 ($x = 0.55$ m, $y = 0.2$ m, $z = 0$ m) of the plate.

The mobilities $M_{12}$, $M_{22}$, $M_{33}$ are determined numerically by a finite element method. One hundred and fifty eigenvalues are calculated for the shell ($\omega_1 = 779$ rad/s, $\omega_{150} = 7052$ rad/s) and for the plate ($\omega_1 = 75$ rad/s, $\omega_{150} = 8453$ rad/s). The mobilities are directly calculated as the ratio between the velocity, provided by the numerical solution
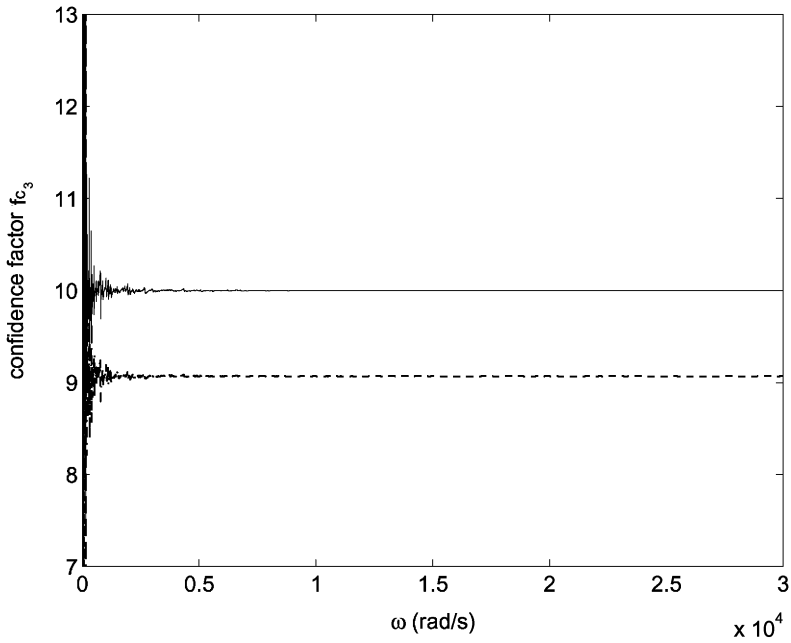
Figure 15. Confidence factor $f_{c_3}$ of the plate–joint with random stiffness–plate system, $k_{G_0} = 1000 \, \text{N/m}$; ——— analytical solution; -.-.-.-.-., Monte-Carlo solution.
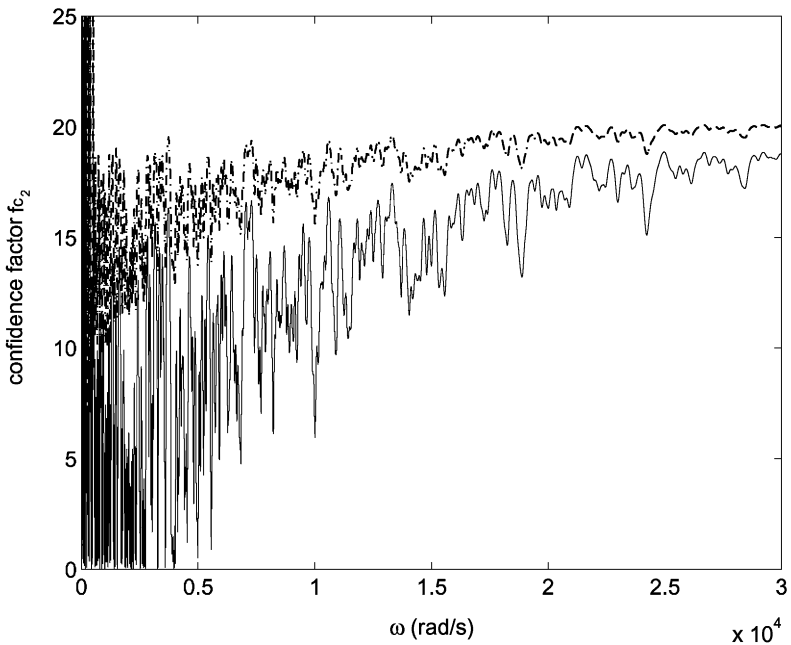


Figure 16. Confidence factor $f_{c_2}$ of the plate–joint with random stiffness–plate system, $k_{G_0} = 10\,000 \, \text{N/m}$; ——, analytical solution; -.-.-.-.-., Monte-Carlo solution.
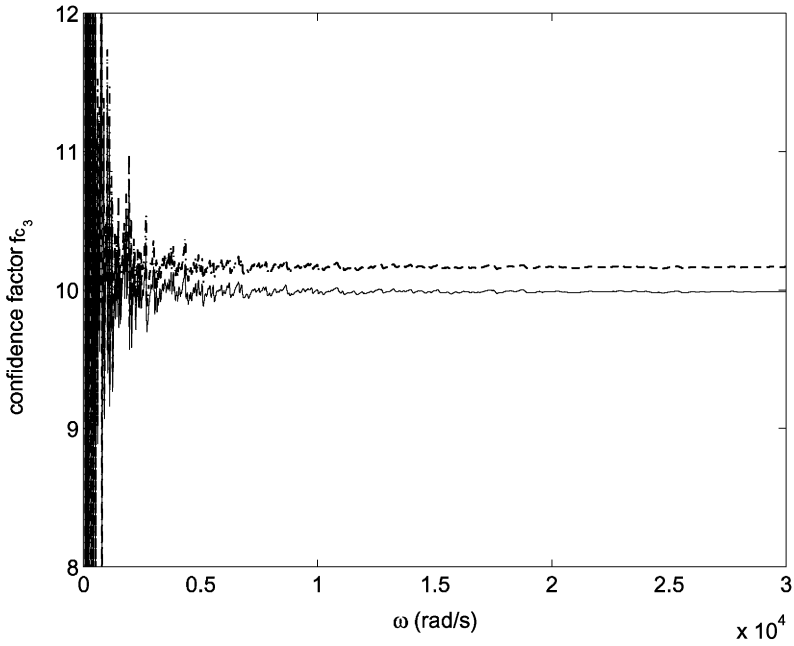
Figure 17. Confidence factor $f_{c_3}$ of the plate–joint with random stiffness–plate system, $k_{G_0} = 10\,000\,\text{N/m}$; ——— analytical solution; -.-.-.-.-., Monte-Carlo solution.

TABLE 9

*Onset of asymptotic trend for two coupled plates*

|              | $k_{G_0} = 1000\,\text{N/m}$ | $k_{G_0} = 10\,000\,\text{N/m}$ |
| ------------ | --------------------------- | ------------------------------ |
| For $f_{c_2}$ | $\omega > 1300$             | $\omega > 4200$                |
| For $f_{c_3}$ | $\omega > 130$              | $\omega > 420$                 |

TABLE 10

*Physical parameters for the shell-plate case*

|       | $E$ (Pa)            | $\rho$ (kg m$^3$) | $h$ (m) | $L_1$ (m) | $L_2$ (m) | $L_3$ (m) | $R$ (m) | $\eta$ |
| ----- | ------------------ | ---------------- | ------- | --------- | --------- | --------- | ------- | ------ |
| Shell | $2.1 \times 10^{11}$ | 7800             | 0.0015  |           |           | 1.2       | 0.7     | 0.01   |
| Plate | $2.1 \times 10^{11}$ | 7800             | 0.0015  | 0.7       | 0.9       |           |         | 0.01   |

of the finite element model, and the force:

$$M_{ij}(\omega) = \frac{v_i(\omega)}{F_j(\omega)}. \tag{64}$$

The value of the joint characteristic, $k_{G_0}$, is equal to $1000\,\text{N/m}$.

The power flows and their statistics are calculated using the numerical values by means of Equations (64),(13), (14) and (20).
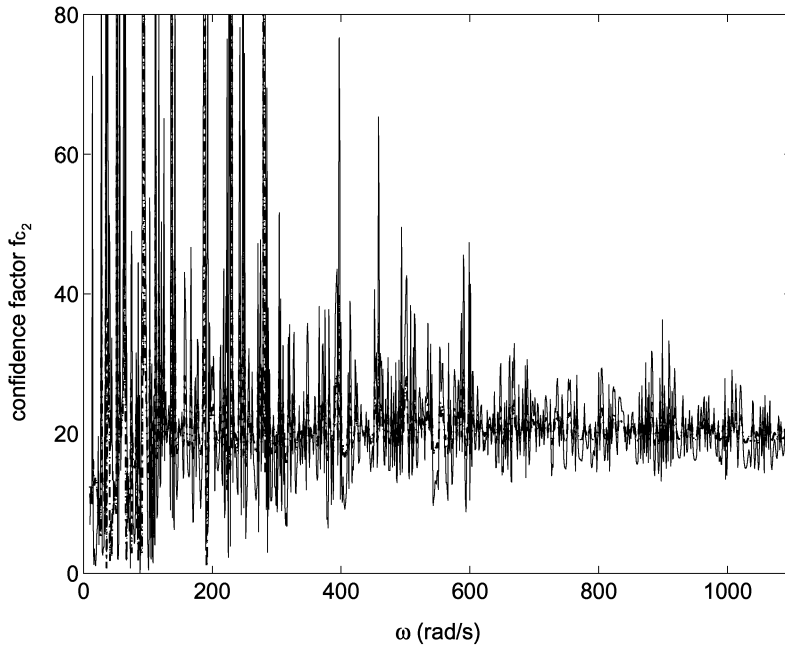
Figure 18. Confidence factor $f_{c_2}$ of the shell–joint with random stiffness–plate system, $k_{G_0} = 1000$ N/m; ——, analytical solution; -.-.-.-.-., Monte-Carlo solution.

Figures 18 and 19 show the confidence factors plotted *vs* frequency. Also in this case it is possible to see the two different frequency regions. In the region between 0 and 1100 Hz the confidence factor $f_{c_2}$ presents an oscillatory behaviour. Beyond 600 Hz , the oscillatory amplitude is very narrow around the value 20 predicted in equation (22). The oscillatory frequency region of the confidence factor $f_{c_3}$ is observed between 0 and 300 Hz, while in the non-oscillatory region the asymptotic value is equal to 10: also in this case equations (22) predict the correct value.

Under conditions (31) and (32) of this numerical example, the constant $\chi$ has not got a defined value. In fact, $\chi = 4$ is correct only for two coupled plates, but it is unknown for a shell. However, using also in this case $\chi = 4$, the graphics of the confidence factors, plotted in Figs 16 and 17, show that this value estimates well the effective condition. The transition frequencies are shown in Table 11.

## 9. REMARKS AND CONCLUSIONS

The present work is aimed to provide a better theoretical understanding of the statistical reliability of an energy flow analysis when random uncertainties in the parameters of the vibrating system are involved. It is expected that this approach adds some important information on the energy flow confidence, that may be used for further developments related to SEA.

An isolated wave guide shows a constant confidence factor, $f_c = 2/\sigma$, which is independent of frequency. The statistics of the power flow are the same at low and high frequency.

If two wave guides are coupled and an incident and a reflected wave propagate along the first one, while only a transmitted wave propagates along the second one, the confidence factor associated with the first wave guide shows a behaviour like that of a single-mode resonator. In a first frequency range the confidence factor presents two peaks, a minimum
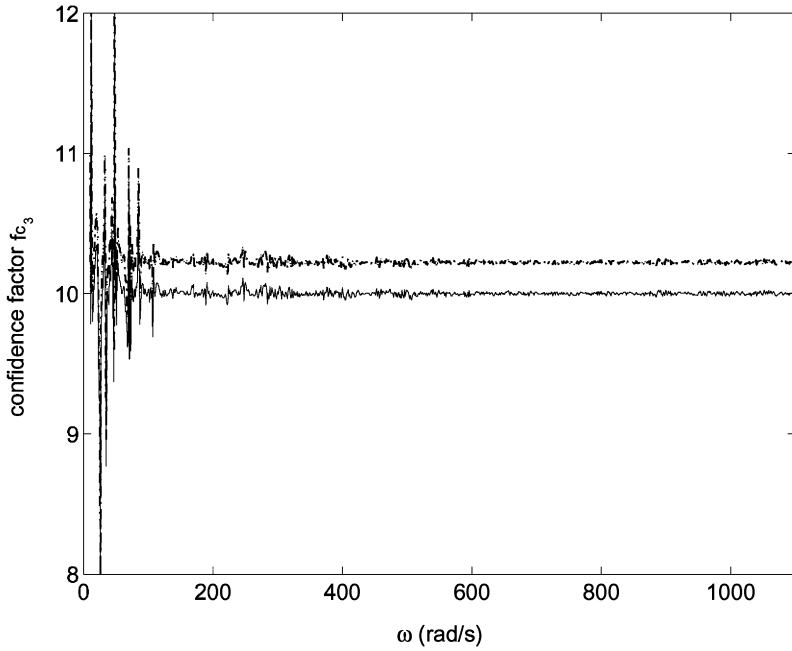
Figure 19. Confidence factor $f_{c_3}$ of the shell–joint with random stiffness–plate system, $k_{G_0} = 1000$ N/m; ——, analytical solution; -.-.-.-.-., Monte-Carlo solution.

TABLE 11

*Onset of asymptotic trend for the shell-plate case*

| | $k_{G_0} = 1000$ N/m |
|---|---|
| For $f_{c_2}$ | $\omega > 2000$ |
| For $f_{c_3}$ | $\omega > 200$ |

and a maximum, respectively; after these peaks the curve tends monotonically to a limit value. The interference between the incident and the reflected waves causes this behaviour in the low-frequency range. In the second wave guide only a single wave propagates and the confidence factors tends monotonically to a constant trend without showing any peak.

When coupling two resonators, a transition frequency appears and an asymptotic limit of the confidence factor exists. The following conclusions can be drawn:

- the greater the coupling the more the asymptotic trend is displaced towards high-frequency values;
- as the coupling strength increases, larger fluctuations of the confidence factor are observed;
- the confidence factor presents peaks in correspondence with the resonances of the two uncoupled subsystems.

It seems clear that any dynamic system, resonator or wave guide, shows an asymptotic constant value of the confidence factor. Before the transition frequency the confidence factor of resonators and coupled wave guides shows a highly oscillating behaviour. Beyond the transition frequency these systems show the same trend of the infinite system.

Although the present analysis is not directly related to SEA and refers to general statistical properties of the energy flows, nevertheless a link with some SEA statements can

be stressed. In fact, the statistics here considered are based on an ensemble average, related to a random joint perturbation, directly performed on an exact expression of the transmitted power flow. This seems not to be the case of SEA, where no statistical moments are formally computed on the energy flow, although occasionally some arguments are developed to account for the randomness of the parameters. Rather, SEA performs explicitly spectral averages on the response of the system subjected to a random excitation. Thus, the results obtained in this paper cannot be transferred directly to SEA.

It is generally recognized that SEA provides a more reliable estimate of the system response for weak coupling and high modal overlap. With these premises it seems reasonable to relate to SEA the asymptotic results here determined. More precisely:

- in the low-frequency region the confidence factor is highly oscillating, implying that the energy flow mean value is not significantly representative of the analysed population at low frequency, but at high frequency only;
- since a weak coupling stabilizes the confidence factor, in that the asymptotic trend is displaced towards the lower frequencies as stated in section 4, the energy flow mean value is more reliable for weak coupling conditions.

## REFERENCES

1. L. CREMER 1953 *Acustica* **3**, 317–335. Calculation of sound propagation in structures.
2. L. CREMER, M. HECKL and E. E. UNGAR 1988 *Structure-Borne Sound.* Berlin: Springer Verlag.
3. M. P. NORTON 1989 *Fundamentals of Noise and Vibration Analysis for Engineers.* Cambridge: Cambridge University Press.
4. F. J. FAHY 1994 *Statistical Energy Analysis: a Critical Overview, in Statistical Energy Analysis.* Cambridge: Cambridge University Press.
5. R. H. LYON and R. G. DE JONG 1995 *Theory and Applications of Statistical Energy Analysis.* Cambridge, MA: The MIT Press.
6. S. DE ROSA, F. FRANCO and F. RICCI 1999 *Introduzione alla Tecnica Statistico-Energetica* (*SEA*). Napoli: Liguori Editore (in Italian).
7. R. H. LYON 1969 *The Journal of the Acoustical Society of America* **45**, 545–565. Statistical analysis of power injection and response in structures and rooms.
8. I. M. SOBOL 1975 *The Monte Carlo Method.* Moscow: MIR Publisher.
9. E. S. VENTSEL 1983 *Teoria delle probabilità.* Mosca: Edizioni MIR. (*in Italian*).
10. M. K. OCHI 1990 *Applied Probability and Stochastic Processes.* New York: John Wiley & Sons.

## APPENDIX A

Let us study the behaviour of the mobility for $\omega \to \infty$. A general expression of the mobility is

$$M_{qr} = \omega\Theta \sum_n \frac{\varphi_n(\zeta_q)\varphi_n(\zeta_r)}{\omega_n^2\eta + j(\omega^2 - \omega_n^2)}$$

where $\Theta$ is a coefficient depending on the system parameter. Let us separate the real and the imaginary parts of the mobility:

$$\mathrm{Re}\{M_{qr}\} = \Theta \sum_n \varphi_n(\zeta_q)\varphi_n(\zeta_r) \frac{\omega\omega_n^2\eta}{\omega_n^4\eta^2 + (\omega^2 - \omega_n^2)^2}$$

$$\mathrm{Im}\{M_{qr}\} = -\Theta \sum_n \varphi_n(\zeta_q)\varphi_n(\zeta_r) \frac{\omega(\omega^2 - \omega_n^2)}{\omega_n^4\eta^2 + (\omega^2 - \omega_n^2)^2}$$

When considering the previous values of the real and imaginary parts for $\omega \to \infty$, we must include the natural frequencies tendency to $\infty$ to guarantee the convergence of the series.

Therefore, by writing explicitly some terms of the series one has

$$\text{Re}\{M_{qr}\} = \Theta\left[\varphi_1(\zeta_q)\varphi_1(\zeta_r)\frac{\omega\omega_1^2\eta}{\omega_1^4\eta^2 + (\omega^2 - \omega_1^2)^2} + \cdots\right.$$

$$+ \varphi_n(\zeta_q)\varphi_n(\zeta_r)\frac{\omega\omega_n^2\eta}{\omega_n^4\eta^2 + (\omega^2 - \omega_n^2)^2} + \cdots$$

$$\left. + \varphi_N(\zeta_q)\varphi_N(\zeta_r)\frac{\omega\omega_N^2\eta}{\omega_N^4\eta^2 + (\omega^2 - \omega_N^2)^2}\right]$$

$$\text{Im}\{M_{qr}\} = -\Theta\left[\varphi_1(\zeta_q)\varphi_1(\zeta_r)\frac{\omega(\omega^2 - \omega_1^2)}{\omega_1^4\eta^2 + (\omega^2 - \omega_1^2)^2} + \cdots\right.$$

$$+ \varphi_n(\zeta_q)\varphi_n(\zeta_r)\frac{\omega(\omega^2 - \omega_n^2)}{\omega_n^4\eta^2 + (\omega^2 - \omega_n^2)^2} + \cdots$$

$$\left. + \varphi_N(\zeta_q)\varphi_N(\zeta_r)\frac{\omega(\omega^2 - \omega_N^2)}{\omega_N^4\eta^2 + (\omega^2 - \omega_N^2)^2}\right].$$

When $\omega$ and $\omega_N \to \infty$, the previous relationships become:

$$\text{Re}\{M_{qr}\} = \Theta\left[\varphi_1(\zeta_q)\varphi_1(\zeta_r)\frac{1}{\omega^3} + \cdots \varphi_n(\zeta_q)\varphi_n(\zeta_r)\frac{1}{\omega^3} + \cdots \varphi_N(\zeta_q)\varphi_N(\zeta_r)\frac{1}{\omega}\right]$$

$$\text{Im}\{M_{qr}\} = -\Theta\left[\varphi_1(\zeta_q)\varphi_1(\zeta_r)\frac{1}{\omega} + \cdots \varphi_n(\zeta_q)\varphi_n(\zeta_r)\frac{1}{\omega} + \cdots \varphi_N(\zeta_q)\varphi_N(\zeta_r)\frac{0}{\omega^3}\right].$$

It is then obvious than both the real and the imaginary part tend to zero as $1/\omega$ so that the modulus of the mobility also tends to zero as $1/\omega$.

## APPENDIX B

B.1. WAVE GUIDE WITH RANDOM YOUNG'S MODULUS

Energy flow is calculated as follows [see equation (37)]:

$$P = \frac{1}{2}\text{Re}\left\{\left(-j\omega S\sqrt{E\rho}\,W\mathrm{e}^{-jk\zeta}\mathrm{e}^{j\omega t}\right)\left(-j\omega W^*\mathrm{e}^{jk\zeta}\mathrm{e}^{-j\omega t}\right)\right\} = -\frac{1}{2}S\omega^2\sqrt{\rho E}|W|^2.$$

The confidence factor [see equation (39)] is

$$fc = \left|\frac{-\frac{1}{2}S\omega^2\sqrt{E_0\rho}|W|^2}{-\frac{1}{4}S\omega^2\sqrt{\frac{\rho}{E_0}}|W|^2 E_0}\right|\left|\frac{1}{\sigma_x}\right|.$$

This is a constant value as indicated in equation (40).

### B.2. RESONATOR WITH RANDOM YOUNG MODULUS

For the sake of simplicity, the calculus is developed by considering a transversely vibrating beam. By equations (41)–(43), the confidence factor can be written as

$$f_c = \left| \frac{\omega\Theta \sum_n \varphi_n(\zeta_q)\varphi_n(\zeta_r)\omega_{n0}^2\eta/(\omega^2 - \omega_{n0}^2)^2}{\omega\Theta \sum_n \varphi_n(\zeta_q)\varphi_n(\zeta_r)[2\eta\omega_{n0}(\omega^2 + \omega_{n0}^2)/(\omega^2 - \omega_{n0}^2)^3](1/2)(n\pi/L)^2\sqrt{(I/E_0\rho S)}E_0} \right| \left\| \frac{1}{\sigma_x} \right|.$$

By simplifying, one obtains

$$f_c = \left| \frac{\sum_n \varphi_n(\zeta_q)\varphi_n(\zeta_r)\omega_{n0}^2\eta/(\omega^2 - \omega_{n0}^2)^2}{\sum_n \varphi_n(\zeta_q)\varphi_n(\zeta_r)[\eta\omega_{n0}(\omega^2 + \omega_{n0}^2)/(\omega^2 - \omega_{n0}^2)^3]\omega_{n0}} \right| \left| \frac{1}{\sigma_x} \right|.$$

As $\omega \to \infty$ the confidence factor behaves as indicated in equation (44).

### B.3. WAVE GUIDE WITH RANDOM YOUNG'S MODULUS COUPLED WITH A RESONATOR

From equations (45) and (46) and the definition of a reflection coefficient, the mobility at $\zeta = 0$ can be calculated as

$$M_0 = \left.\frac{\dot{w}}{N}\right|_{\zeta=0} = \left.\frac{j\omega(W^i + W^r)e^{j\omega t}}{j\omega S\sqrt{E\rho}(W^i - W^r)e^{j\omega t}}\right|_{\zeta=0} = \frac{1+r}{S\sqrt{E\rho}(1-r)}$$

and the reflection coefficient is

$$r = -\frac{1 - S\sqrt{E\rho}M_0}{1 + S\sqrt{E\rho}M_0}.$$

By using the following relationships

$$\alpha = -1 + S\sqrt{E\rho}\,\text{Re}\{M_0\}, \quad \beta = 1 + S\sqrt{E\rho}\,\text{Re}\{M_0\}, \quad \gamma = S\sqrt{E\rho}\,\text{Im}\{M_0\}$$

the modulus squared of the reflection coefficient [see equation (47)] is

$$|r|^2 = \frac{(\alpha\beta + \gamma^2)^2 + (\beta - \alpha)^2\gamma^2}{(\beta^2 + \gamma^2)^2}$$

while the confidence factor becomes

$$fc = \left| \frac{\sqrt{E\rho}\left(1 + S^2E\rho(\text{Im}\{M_0\}^2 + \text{Re}\{M_0\}^2) + 2\text{Re}\{M_0\}S\sqrt{E\rho}\right)}{\text{Re}\{M_0\}SE\rho + \sqrt{E\rho}} \right| \left| \frac{1}{\sigma_x} \right|.$$

### B.4. WAVE GUIDE–JOINT WITH RANDOM STIFFNESS–WAVE GUIDE

Figure 20 shows the behaviours of the two confidence factors of equations (57). The test case is: two equal semi-infinite rods ($E_1 = E_2 = 2.1 \times 10^{11}$ Pa, $\rho_1 = \rho_2 = 7800$ kg m$^3$, $S_1 = S_2 = 1 \times 10^{-4}$ m$^2$, $k_{G0} = 1000$ N/m, $\eta = 0.01$, $\sigma_x = 0.05$). The values predicted by equations (58) and (59) are reached.

## APPENDIX C

Let us consider the equations of the powers $P_2$ and $P_3$ represented in the simpler form

$$P_3 = \frac{\alpha}{2\delta}\frac{N_3(x)}{D(x)}, \quad P_2 = -P_3 - \frac{\mu\eta\omega}{2k_{G_0}\delta}\frac{N_2(x)}{D(x)}$$
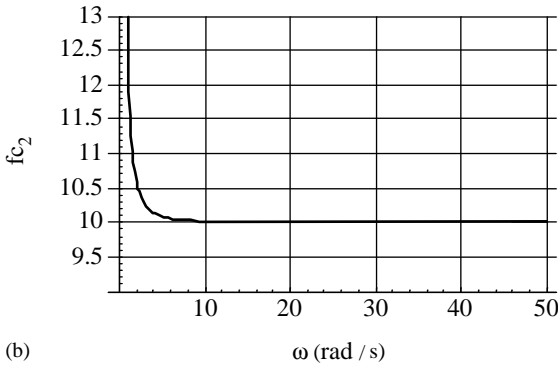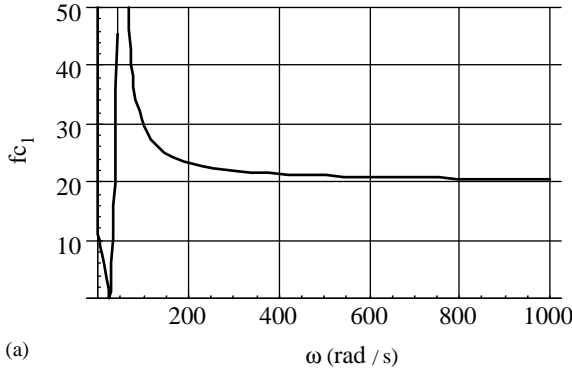
Figure 20.  Waveguide-random joint-wave, $a$; Confidence factor $f_{c_1}$ $b$: Confidence $f_{c_2}$.

with obvious meaning of symbols. Their derivatives are

$$\frac{\partial P_3}{\partial x} = \frac{\alpha}{2\delta} \frac{N_3'D - N_3 D'}{D}, \quad \frac{\partial P_2}{\partial x} = -\frac{\partial P_3}{\partial x} - \frac{\mu\eta\omega}{2k_{G_0}\delta} \frac{N_2'D - N_2 D'}{D}.$$

Thus in order to perform a series expansion, it is necessary that

$$\left.\frac{\partial P_i}{\partial x}\right|_{x=0} < \infty, \ i = 2, 3.$$

Since $\delta \neq 0$, it implies

$$D(x)|_{x=0} \neq 0$$

or explicitly

$$\frac{k_{G_0}^2 \chi^2}{m\omega^2}(\tilde\beta^2 + \tilde\gamma^2) + \omega^2 \neq 2\frac{k_{G_0}\chi}{m}(\tilde\beta\eta + \tilde\gamma). \tag{C1}$$

Let us introduce the associated inequality

$$\frac{k_{G_0}^2 \chi^2}{m\omega^2}(\tilde\beta^2 + \tilde\gamma^2) + \omega^2 > 2\frac{k_{G_0}\chi}{m}(\tilde\beta\eta + \tilde\gamma) \tag{C2}$$

that implies, necessarily, condition (65).

We are interested to determine a frequency range in which inequality (66) is satisfied. To this aim, considering: the following condition:

$$\tilde{\beta} = \text{Re}\{\tilde{M}_{33}\} + \text{Re}\{\tilde{M}_{22}\} \tag{C3}$$

let us modify inequality (66) as follows:

$$\frac{k_{G_0}^2 \chi^2}{m\omega^2}(\tilde{\beta}^2 + \tilde{\gamma}^2) + \omega^2 > 2\frac{k_{G_0}\chi}{m}(|\tilde{\beta}|\eta + |\tilde{\gamma}|) > 2\frac{k_{G_0}\chi}{m}(\tilde{\beta}\eta + \tilde{\gamma}). \tag{C4}$$

Considering that

$$\text{Re}\{\tilde{M}_{ij}\} = \sum_n \frac{\phi_{ni}\phi_{nj}\tilde{\omega}_n^2\eta}{\tilde{\omega}_n^4\eta^2 + (1 - \tilde{\omega}_n^2)^2}$$

the highest value of each contribution in the previous sum is found in correspondence of the associated resonance. Therefore,

$$\text{Re}\{\tilde{M}_{ij}\} \leqslant \sum_n \left|\frac{\phi_{ni}\phi_{nj}}{\eta}\right| \leqslant \sum_n \frac{|\phi_{ni}||\phi_{nj}|}{\eta} \leqslant \sum_n \frac{A}{\eta}$$

where $A = \max\{\phi_{ni}^2\}$. If $N(\omega)$ is the total number of modes within the frequency band $[0, \omega]$, one has

$$\text{Re}\{\tilde{M}_{ij}\} \leqslant \sum_n \frac{N(\omega)A}{\eta}$$

Thus, considering equation (67), it follows:

$$0 \leqslant |\tilde{\beta}| \leqslant \frac{N_{\text{II}}(\omega)A_{\text{II}}}{\eta_{\text{II}}} + \frac{N_{\text{I}}(\omega)A_{\text{I}}}{\eta_{\text{I}}}. \tag{C5}$$

By proceeding in a similar way for $\tilde{\gamma}$, one obtains

$$0 \leqslant |\tilde{\gamma}| \leqslant \omega B_{\text{I}}\eta_{\text{I}}(\omega) + \omega B_{\text{II}}\eta_{\text{II}}(\omega). \tag{C6}$$

The condition

$$\frac{k_{G_0}^2 \chi^2}{m\omega^2}(\tilde{\beta}^2 + \tilde{\gamma}^2)_{\text{MIN}} + \omega^2 > 2\frac{k_{G_0}\chi}{m}(|\tilde{\beta}|\eta + |\tilde{\gamma}|)_{\text{MAX}} \tag{C7}$$

implies equation (C7). Thus, the following relationship is obtained:

$$\omega^2 > 2\frac{k_{G_0}\chi}{m}\left[\frac{A_{\text{II}}\eta}{\eta_{\text{II}}}\int_0^\omega n_{\text{II}}(v)\,\mathrm{d}v + \frac{A_{\text{I}}\eta}{\eta_{\text{I}}}\int_0^\omega n_{\text{I}}(v)dv + B_{\text{II}}\omega n_{\text{II}} + B_{\text{I}}\omega n_{\text{I}}\right]$$

and choosing $n(\omega) = \alpha\omega^m$, it becomes

$$\omega^2 > 2\frac{k_{G_0}\chi}{m}\left[\frac{A_{\text{II}}\eta}{\eta_{\text{II}}}\frac{\alpha_{\text{II}}\omega^{m_{\text{II}}+1}}{m_{\text{II}}+1} + \frac{A_{\text{I}}\eta}{\eta_{\text{I}}}\frac{\alpha_{\text{I}}\omega^{m_{\text{I}}+1}}{m_{\text{I}}+1} + B_{\text{II}}\omega^{m_{\text{II}}+1} + B_{\text{I}}\omega m_{\text{II}} + 1\right]$$

For the following cases we have

- longitudinal beam: $m = 0$
- flexural beam: $m = -1/2$
- flexural plate: $m = 0$

so that for these structures the trend of the right-hand side in the last equation increases less than $\omega^2$. As $\omega \to \infty$ the condition is verified.